

Gaia's Crown: A Deep Space Mirage

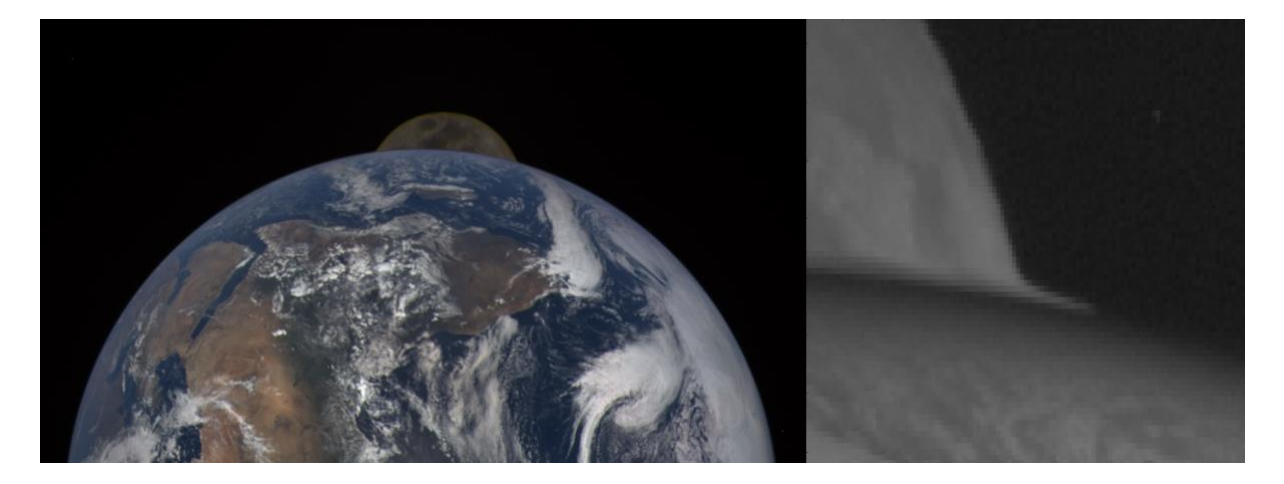
- 1 Karin Blank¹, Jay Herman^{1,2}, Sarah Dangelo¹, Alexander Marshak¹, Andrew Tennenbaum¹
- ¹Goddard Space Flight Center, NASA, Greenbelt, Maryland, United States
- ²University of Maryland Baltimore County, Baltimore, Maryland, United States
- 4 Keywords: DSCOVR, EPIC, atmospheric optics, mirage
- 5 Abstract
- 6 The Earth Polychromatic Imaging Camera (EPIC), onboard the Deep Space Climate Observatory
- 7 (DSCOVR) spacecraft, has captured a unique optical effect during lunar occultation named "Gaia's
- 8 Crown". This phenomenon, observable in the infrared and visible channels, but not in the ultraviolet,
- 9 is seen as a flange between the Earth and the Moon when the two visually intersect. Using
- atmospheric data and 3D, voxel-based ray tracing models, this effect was identified as a combination
- of atmospheric distortion and a complex mirage caused by variations in the Earth's atmosphere.
- 12 Additionally, it is shown that satellites closer to the Earth cannot see this phenomenon and
- demonstrates how EPIC's vantage point at 1.5 million kilometers provides a unique perspective on
- 14 atmospheric optics.

15 1 Introduction

- 16 The Deep Space Climate Observatory (DSCOVR) is a NOAA-operated satellite that orbits the Earth-
- 17 Sun Lagrange-1 (L1) point. This location, approximately 1.5 million kilometers away from the Earth,
- offers a unique view of the planet where the disk is almost fully illuminated. The DSCOVR
- spacecraft serves as a host to both Sun and Earth-observing instruments.
- 20 The Earth Polychromatic Imaging Camera, a NASA instrument onboard DSCOVR, utilizes a 30cm
- 21 Cassegrain telescope to photograph the Earth from this vantage point. Utilizing a 2048x2048 charge-
- coupled device (CCD) sensor, it takes 13 or 22 image sets daily, in a set of 10 narrow bands between
- 23 317-780nm wavelength, with the more frequent sets occurring during the Northern Hemisphere
- summer. This wavelength range permits a unique view of the Earth in ultraviolet, visible, and
- 25 infrared which enables detection of ozone, sulfur dioxide, aerosols, vegetation, ocean, cloud
- properties, and other science applications (Marshak, 2018).

2 Observations

- 28 The EPIC camera nominally observes just the sunlit Earth, but its 0.62° field of view permits a view
- 29 that occasionally includes the Moon as well, as seen in the left portion of *Figure 1*. The instrument
- 30 observes these events roughly 4 times a year 2 with the Moon passing in front of the Earth and the
- 31 remainder with it passing behind.

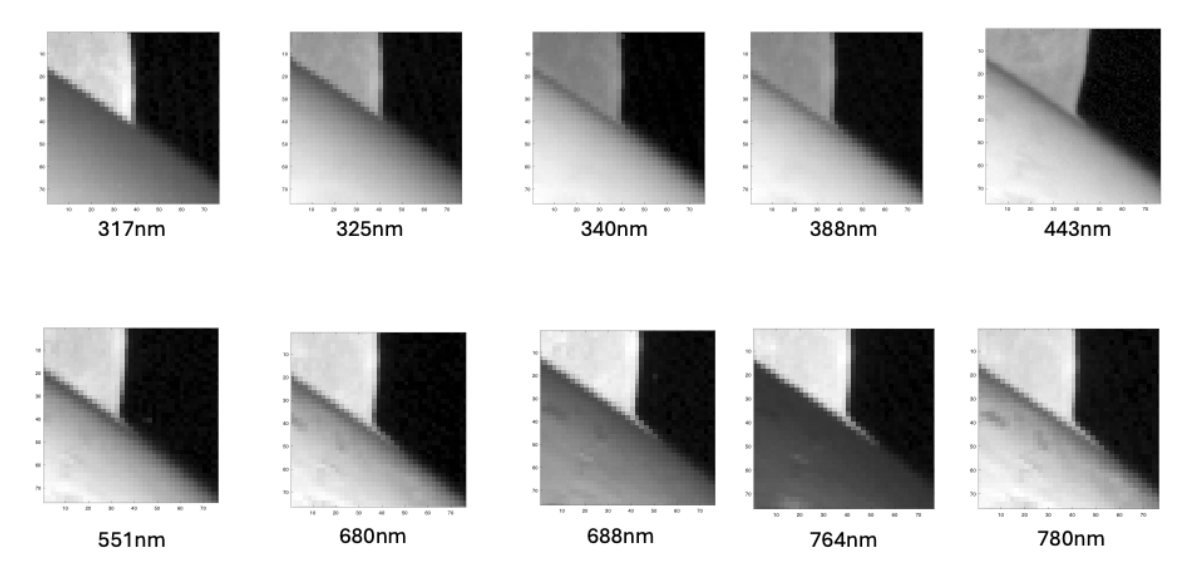


33

Figure 1 - Left: Color image taken by EPIC of the Moon passing behind the Earth taken on September 27, 2015. Right: A zoom in of the 680nm band that shows the "flange effect" where the Moon intersects with the Earth. Image gamma corrected to improve visibility of phenomenon.

- 37 In 2015, a special imaging was performed where the EPIC camera was trained upon the Moon,
- following it as it transited behind the Earth. Upon more detailed inspection of the images, an
- interesting effect was seen as the Moon passed behind the Earth. In this sequence, as seen in the
- right, zoomed in portion of Figure 1, a small "flange" is seen, appearing as almost a mount for the
- 41 Moon against the planet's surface. It was not known what this phenomenon was or what it originated
- from. This paper will discuss the origin of the phenomenon and the underlying optics.
- 43 A review of the original, unprocessed level 0 data also revealed the feature, eliminating possible
- calibration artifacts as the cause. The pixels in the feature are not saturated, indicating the cause is not
- 45 CCD bloom, nor does it mimic any known optical artifact of the telescope.
- Because the sequence was part of a public outreach imaging to acquire color photos of the Moon
- passing behind the Earth's disk, the instrument recorded only the red (680nm), green (551nm), and
- blue (443nm) channels. The phenomenon was seen in all 3 wavelengths.
- 49 A review of the EPIC archive was conducted and all images where the Moon passed behind the Earth
- were obtained. Out of the 16 image sets obtained where the Moon intersected the Earth's horizon,
- only one other set contained the flange effect. Based on this, the effect appeared to only be occurring
- 52 under certain conditions.
- In an additional dataset, all ten bands were obtained (*Figure 2*), enabling a view of the flange effect
- 54 in different wavelengths. The phenomenon is mostly invisible in ultraviolet (UV) bands 317, 325,
- 340, and 388nm and becomes increasingly clearer as the bands progress through 443, 551, 680, 688,
- 56 764, and 780nm. This indicates that the phenomenon is not likely due to atmospheric scattering,
- 57 which is smaller in the visible and near-IR bands (*Figure* 2).

Phenomenon at different wavelengths



epic_1a_20201130170738_03.h5

Figure 2 - Flange phenomenon in different wavelengths. From data taken November 11th, 2020.

Inspection of the Moon passing behind the Earth from two other spacecraft, as seen in *Figure 3*, did not yield the same phenomenon. Both images from the International Space Station (ISS) and Geostationary Operational Environmental Satellite (GOES) Advanced Baseline Imager (ABI) display expected optical compression from refraction through the atmosphere. This optical compression can also be seen in images from Himawari-8 (Universe Space Tech, 2023).



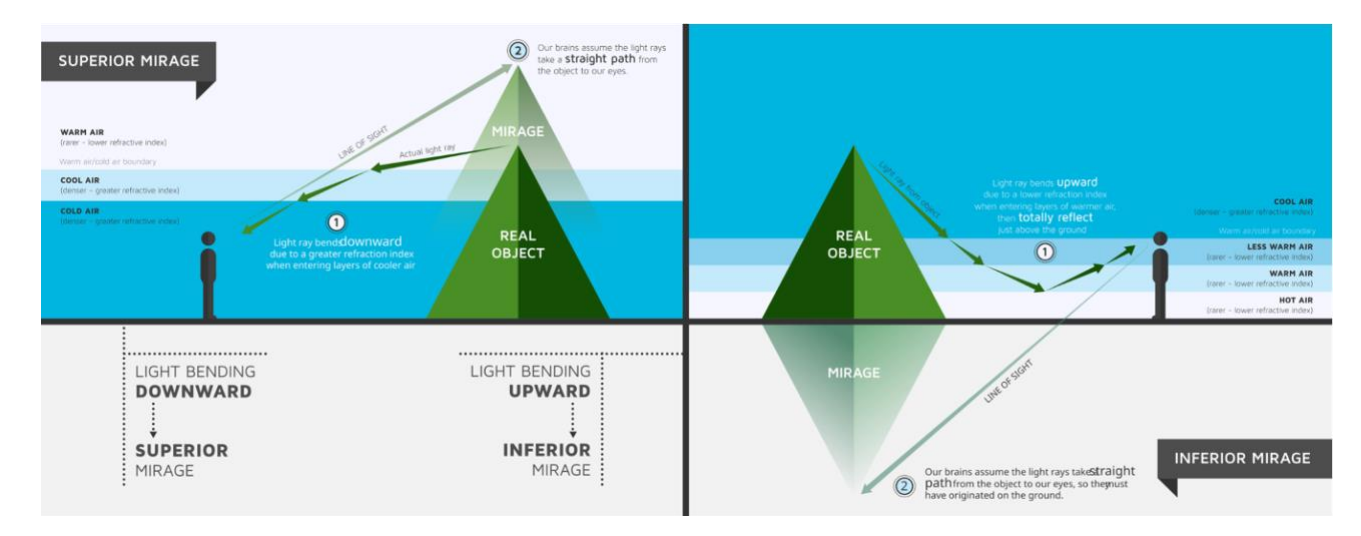
Figure 3 - Views of Moon rising from Earth. Left astronaut photography from International Space Station (ISS) (NASA via Astronomy.com, 2023). Right from GOES Advanced Baseline Imager (ABI) (NOAA, 2020). Both exhibit typical optical compression from atmospheric distortion.

Mirage Review



Figure 4 - Example of Sun "omega mirage". This inferior mirage occurs when the ocean creates a surface of low-density hot air. (Inaglory, 2007)

- At this point, a further review of atmospheric phenomenon was conducted, and from the catalogue of possible features, the following conclusion was derived: that this was very similar to a feature known as an "omega mirage".
- Mirages are an optical phenomenon where light is bent by different, contrasting combinations of air temperatures and humidity. This bending, produced by different refractive indices of the layers, causes displacement and distortion of distant objects in the sky.



80

Figure 5 – Examples of superior and inferior mirages. (Lorenzelli, 2014)

- 81 Mirages are separated into roughly three classes: inferior, superior, and "complex".
- In inferior mirages, as seen in *Figure* 5 on the left, an inversion of the light rays causes a mirror reflection of an object to appear below it. This is caused by scenarios where high temperatures are near the ground followed by layers of cooler temperatures as the air gets away from the ground. A common example of this is the "highway mirage" where a hot road appears as if it has a reflective puddle, but instead it is caused by the temperature differences above the road.
- 87 In superior mirages, as seen in *Figure* 5 on the right, light bends in such a way to cause an object to 88 appear float above its original location. In this situation, layers of cool air followed by warm cause an 89 expansion effect, which makes the objects appear higher. Superior mirages often cause objects that

- are visually below the line of sight, appear on the horizon when they, in normal conditions, would
- 91 not.
- The final mirage, a "complex mirage", is caused when there are alternating layers between hot and
- 93 cold air. In these mirages, known as fata morgana, the optical effects consist of inverted images,
- ompressed and stretched layers, as well as objects "floating" on the horizon (Siebren van der Werf,
- 95 2022).

4 Theory Development

- 97 Terrestrial mirages occur when different temperature layers cause changes in the air density, which
- leads to changes in the refractive index. Near the ground, these thermal layers are due to local
- onditions; heat rising from the ocean or cool air, followed by warm, creates different optical
- 100 distortions.
- 101 It was considered that this flange effect was perhaps based on atmospheric conditions. Goddard Earth
- 102 Observing System (GEOS) data, which models atmospheric parameters including temperature and
- humidity, were obtained and reprojected into the EPIC projection and field of view at the times of
- 104 EPIC partial lunar occultation events. However, the results revealed no evidence of a relationship
- between temporal atmospheric conditions and whether the flange effect appeared.
- Further review of the data was conducted, and it was observed that the two times the phenomenon
- was observed was when the Moon was halfway below the horizon. Based on this, a new hypothesis
- was formed: that this phenomenon was not fleeting but occurred every time the Moon passed behind
- the Earth and occurred while the Moon was at least halfway below the horizon.
- 110 Under the assumption that this is a consistent event, we propose a new hypothesis. The atmospheric
- layers, while generally characterized by a decrease in temperatures with an increase of altitude, do
- not do this in a linear fashion. Instead, there is a switching back and forth of the temperature as
- altitude increases. The troposphere, stratosphere, mesosphere, and thermosphere are characterized by
- alternating cooling and rising temperatures. These different layers create a ripe environment for
- mirage-type optical distortion by providing contrasting refractive indices.

116 **5 Methods**

123

- There are many ways to model the effect of atmospheric distortion on light. Common astronomical
- methods use heuristics as a function of viewing angle. Many, including the EPIC geolocation
- algorithm (Blank, 2019), use layer-based raytracing models that treat the atmosphere as a linear, 2-
- dimensional pathway. However, these common methods had not revealed any type of optical
- phenomenon, other than compression, at distance. If the phenomenon is a mirage, resolving it
- requires a fully three-dimensional model rather than the usual 2D approximations.

5.1 Raytracer Model Overview

- To this end, a voxel-based raytracer utilizing vectors was developed. Raytracers are software which
- estimates the path of viewing rays in a virtual scene. Voxels, a portmanteau of "volumetric pixel", are
- essentially 3D pixels, where each voxel is populated with a property. In this case, the property is the
- refractive index of a physical location. Using vector math permits a complete 3D calculation of the
- ray paths and interactions with the Earth's atmosphere, determining how the rays are warped and
- where they intersect with the Moon. Furthermore, unlike most raytracers that discard the

intermediary products, a secondary voxel model can store all computed vectors and distortion levels, permitting inspection of the actual phenomenon on post processing.

130

131

133

134

135

139

140

141 142

143

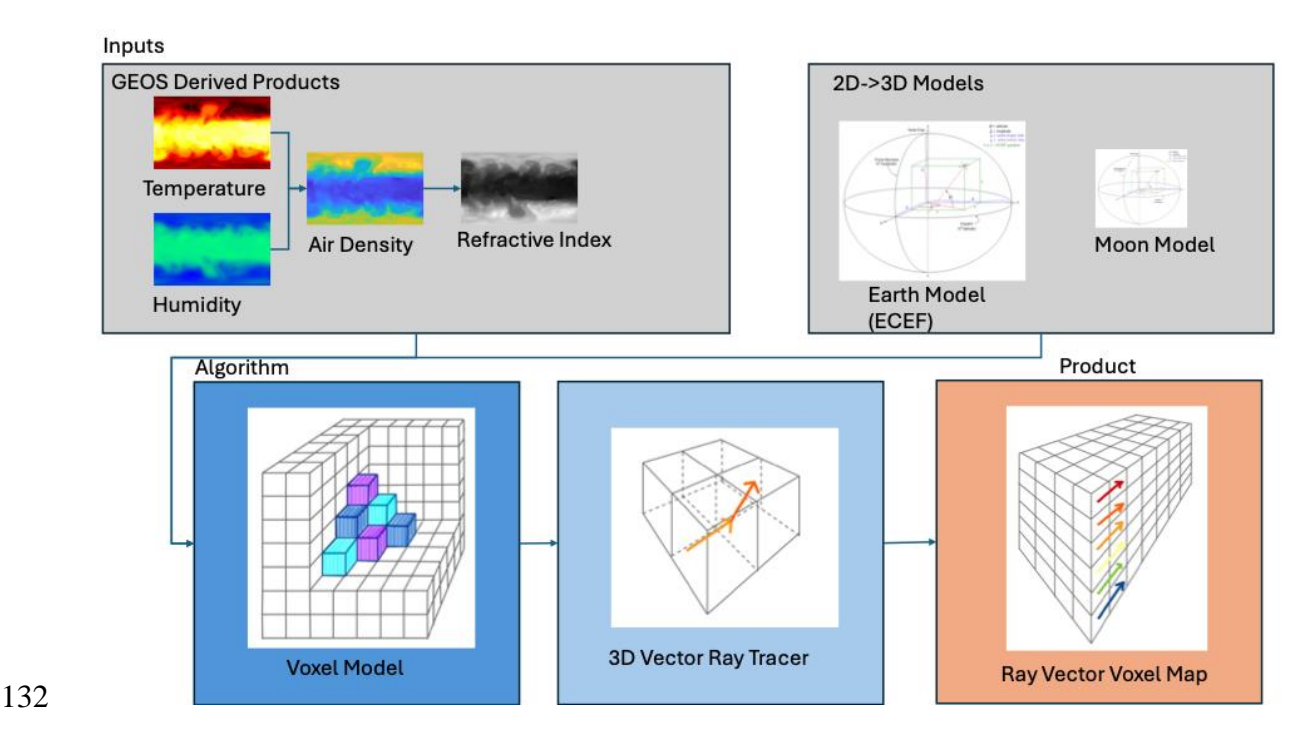


Figure 6 - Voxel raytracer pipeline. GEOS data is used to derive the refractive indices, which are then combined with geophysical models and used to populate the voxel model. The 3D vector based raytracer then calculates optical paths and stores the results the ray vector voxel map.

- A basic renderer (*Figure 6*) would consist of GEOS-derived refractive indices and an Earth and Moon model which would be used to populate a voxel model. The vector-based ray tracer would then compute on top of the model, producing vector voxel maps of the resulting view rays.
 - However, this is not without challenge. A full model of the EPIC, Earth, and Moon space, consisting of these refractive voxels, has a computational and storage complexity of O(n³) where n is a function of resolution. EPIC has a resolution of ~8km, but to get a clear ray paths for a potential mirage, which might contain ray inversions, requires a voxel space that is oversampled by 3-4x. A basic calculation of a 2 km voxel model of the Earth/Moon scene from EPIC would have a volume of ~10.8 trillion km³ or ~5.4 trillion voxels. On a computer, using double precision floating point, this would require over 43 petabytes of memory, an impractical amount.
- To improve resource utilization, a "just-in-time" renderer was developed. In this paradigm, only the portions of the scene that are immediately being computed upon are rendered. A further reduction in computation is obtained by clipping the rendered scene to a subset of the optical pathways needed for the optical effect.
- The renderer is prepared by developing abstract models that contain the values needed, but not in the voxel format. Data from GEOS, including pressure, temperature, and humidity for each atmospheric layer, is ingested in equirectangular projection and the air density and subsequent refractive index are calculated. An abstract 3D model of the Earth and the Moon, in Earth-Centered, Earth-Fixed (ECEF) (Nishihama, 1997) XYZ coordinates is also separately computed.

1	5	4
1	J	J

- During computation, instead of having the entire voxel model precomputed, one slice along the X
- axis is rendered at a time. The abstract models are used to generate look-up indices into the
- equirectangular refraction datasets, and these values are pulled into a 2D, YZ-dimension slice. The
- vector renderer then calculates the resulting angular distortions from refraction and the new ray-
- vectors, along with distorted YZ index offsets, which are then stored in an HDF (hierarchical data
- format) file. If an opaque surface is encountered, or the calculation yields a reflection, the ray is
- "snipped", and no more computations occur on it. The renderer marches through the model space,
- one slice at a time, until it reaches the end.
- In sections where there is only the vacuum of space, such as between the Earth and the Moon, the
- renderer will skip drawing ray slices and compute new YZ index offsets based on the distances
- 166 covered.
- The product of the raytracer is a full 3D map of the viewing rays' vectors and the amount of
- distortion per ray, stored in HDF format. Making this data useful requires additional software that
- can pull the relative data and put it in a viewable format.

5.2 Refractive Index Computation

- To calculate refraction, the GEOS model "inst3 3d asm Np", which contains 3D assimilated states
- at various pressure levels, is used. There are 42 layers in this set, each at a different pressure level,
- 173 covering altitudes from sea level to ~65km. Each layer contains, in equirectangular projection, values
- for temperature, humidity, and pressure from which the air density and refractive index can be
- 175 derived.

176

170

- 177 The process for calculating air density is essentially to derive the amount of dry air versus water
- vapor (Omnicalculator, 2024). The first step is to calculate saturation vapor pressure, *svp*, via Tetens
- equation (Wikipeida, Tetens). T is the temperature in Celsius, and RH is the relative humidity, both
- obtained from the GEOS model.

181

182
$$svp = 0.61078 * \exp\left(\frac{17.27T}{T + 237.2}\right)$$

183 Actual vapor pressure (*avp*) is then:

$$avp = svp * RH$$

185

Pressure (P), in units of kPa, is then used to estimate the dry air pressure, dap, (kPa) via:

$$dap = P - avp$$

Using 287.058 J/(kg K) as the specific gas constant for dry air, and 461.495 J/(kg K) as the specific gas constant for water vapor, the air density can be calculated via:

192

193
$$airdens = \frac{1000 * dap}{287.058 * T} + \frac{1000 * avp}{461.495 * T}$$

194

The refractive index (*refindex*) for visible light is then calculated as follows, where 1.29 kg/m³ is the air density at room temperature and pressure and c is the speed of light in m/s.

197

198
$$refindex = \frac{c}{c * (1 - .00029 * \left(\frac{airdens}{1.29}\right))}$$

199

- 200 This calculation is done for each layer of the GEOS dataset. The framework for these calculations
- 201 was derived from OmniCalculator

202 **5.2.1 Vector Raytracer**

- Refraction is modelled with Snell's law (Angel, 2000), which describes that when a ray encounters a
- surface with a different index of refraction, the angle that the light gets transmitted through the
- surface is dependent on the ratio between the current and new refractive indices, as well as the angle
- of incidence. Essentially:

$$\frac{\sin(\Theta_l)}{\sin(\Theta_t)} = \frac{n_t}{n_l}$$

- Where Θ_l and Θ_t are the incident and transmitted angle; n_l and n_t are the refractive indices for
- 209 current and new surface.
- 210 To apply this property to vectors requires some adaptation. Two vectors are needed, one of which is
- 211 the vector representing the current ray, defined as v_r. The second is for the voxel coordinate of the
- 212 atmospheric surface with which the ray vector is colliding. This vector is from the Earth's center
- 213 coordinate to the current voxel coordinate and is defined as v_a.
- The intersection angle, Θ_l , between the two vectors is computed:

$$\Theta_l = \cos^{-1}(v_a \cdot v_r)$$

216 The ratio between refractive indices is:

$$217 n = \frac{n_t}{n_l}$$

And the angle the light is refracted is:

$$\Theta_t = \cos^{-1} \left(1 - \frac{1}{n^2} * (1 - (\cos(\Theta_l)^2))^{0.5} \right)$$

To calculate the refracted vector, v_t , is then:

$$v_t = -\frac{1}{n}v_l - (\cos(\theta_t) - \frac{1}{n}\cos(\theta_l))v_a$$

- If Θ_t is a complex number, the ray is encountering the critical angle and being reflected instead of
- transmitted. In this case, the program snips the ray as it is no longer propagated through the model.
- Rays are also snipped when they encounter a non-transparent surface, such as the surface of the Earth
- or the Moon.
- The amount of distortion for each ray is tracked and updated through each propagation.
- The magnitude factor of each ray is calculated by normalizing the x component transmitted vector,
- since the algorithm can only advance the rays on discrete slices:

$$f = \frac{1}{v_{tx}}$$

230 Where the new coordinates are:

$$x_{n+1} = x_n + v_{tx} * f$$

$$y_{n+1} = y_n + v_{ty} * f$$

$$z_{n+1} = z_n + v_{tz} * f$$

- Note that the x calculation can be skipped since it will always advance by 1 due to the discrete nature
- of the voxel model; it is left here for completeness.
- The initial ray vector slice that starts the process is calculated based on the field of view (FOV) of the
- 237 instrument. Where the FOV angle is φ , F is the maximum vector.

$$F = \frac{\sin(\varphi)}{2}$$

239 The rate of change across the slice is calculated, where vol is the voxel model dimensions in the y

240 and z axis:

$$\Delta y = \frac{2F}{vol_{\nu}}$$

$$\Delta z = \frac{2F}{vol_z}$$

244 Then each ray vector for the initialization slice is calculated, where i is the column and j is the row, 245 and *init* is the initial ray slice: $init_y_{ij} = -F + \Delta y * i$ 246 247 $init_z_{ij} = -F + \Delta z * i$ 248 249 250 5.3 Putting it all together 251 The raytracer comes together in the following steps: 252 1) The initial parameters for the voxel model are setup according to the scene, and dimensions are determined by the locations of the Earth and the Moon and the voxel resolution. 253 254 2) The GEOS dataset is ingested and the refractive indices for the atmospheric layers are calculated. If necessary, neighboring layers can be averaged together to meet the resolution of 255 256 the voxel model. 3) The initial ray vector states are calculated, based on the FOV angle. This becomes the current 257 258 ray vector. 4) The raytracer then runs iteratively through the voxel model, advancing forward slice by slice 259 260 until it reaches the end. This consists of the following steps: 261 The current slice is drawn by pulling the relevant refractive indices from the layer 262 model into their proper location in the slice. b. The Earth's center coordinate to the current slice coordinate is built and the algorithm 263 264 for calculating the transmitted angle is executed. Any rays that are reflected or encounter a body are snipped. If a body is encountered, the type is stored (i.e. Earth vs 265 Moon). 266 267 c. The amount of distortion for each ray is calculated. d. Data concerning the ray vectors, refraction, angle of incidence, and transmitted angles 268 are stored in a file for future analysis. 269 270 5) The final simulated image is calculated based on the states of the ray vectors and the 271 calculated level of distortion. 272

273 6 Results

The raytracer was run at 2km resolution, resulting in *Figure 7* and *Figure 8*. As seen in the ray traced image compared to the actual image from EPIC, the same phenomenon is seen. A vertical sampling of the rays reveals a maximum 0.45° distortion that decreases with distance away from the Earth.

This is not unexpected, as the refractive indices decrease in relation to the air density, but it is interesting to note that the descent has several "bumps" where it increases instead of decreases.

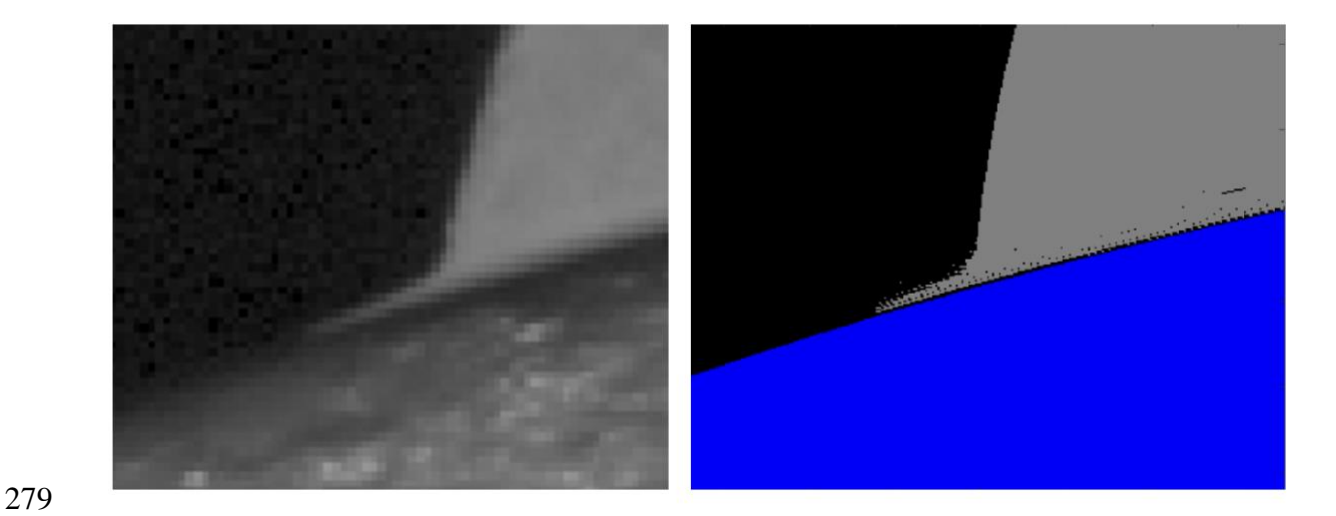


Figure 7 - Left: EPIC image of the Moon "flange" effect. Right: Results from raytracer. Because this model uses discrete rays, small black dots occur where there is no ray present due to diversion from refraction

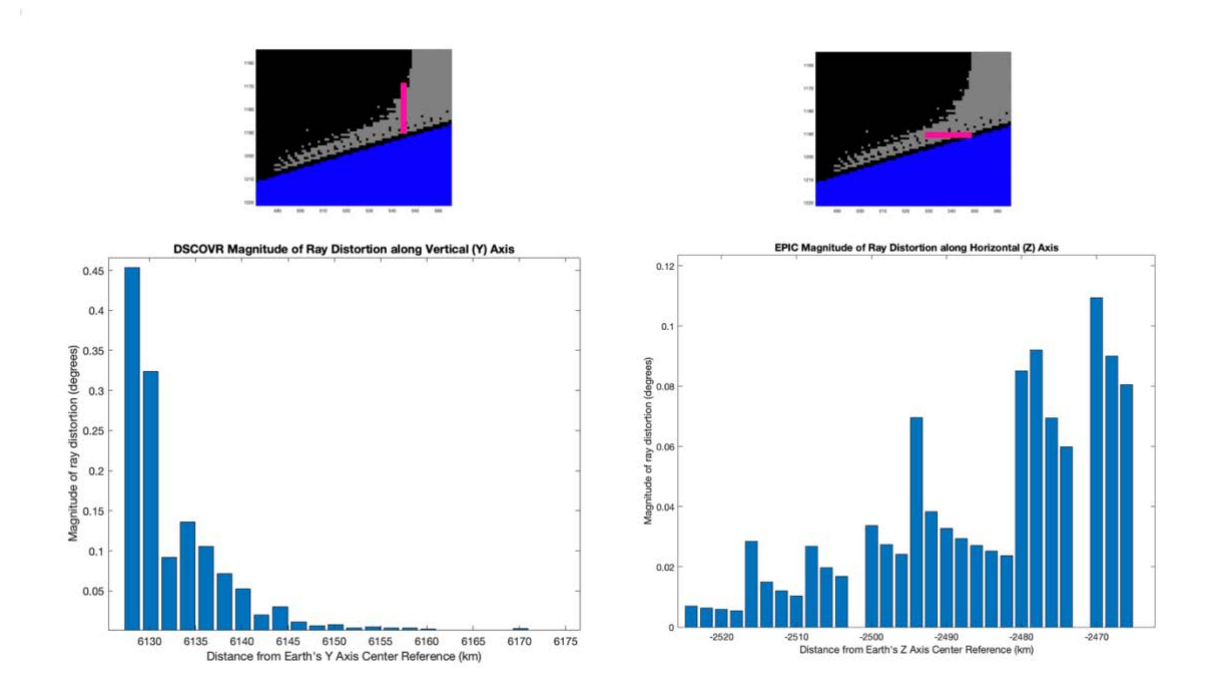


Figure 8 - Left: Per ray magnitude of distortion along vertical axis. Right: Per ray magnitude of distortion along horizontal axis

An inspection of the rays as they traverse through the atmosphere (*Figure 9*) shows that the rays are primarily traveling through the stratosphere and lower mesosphere.

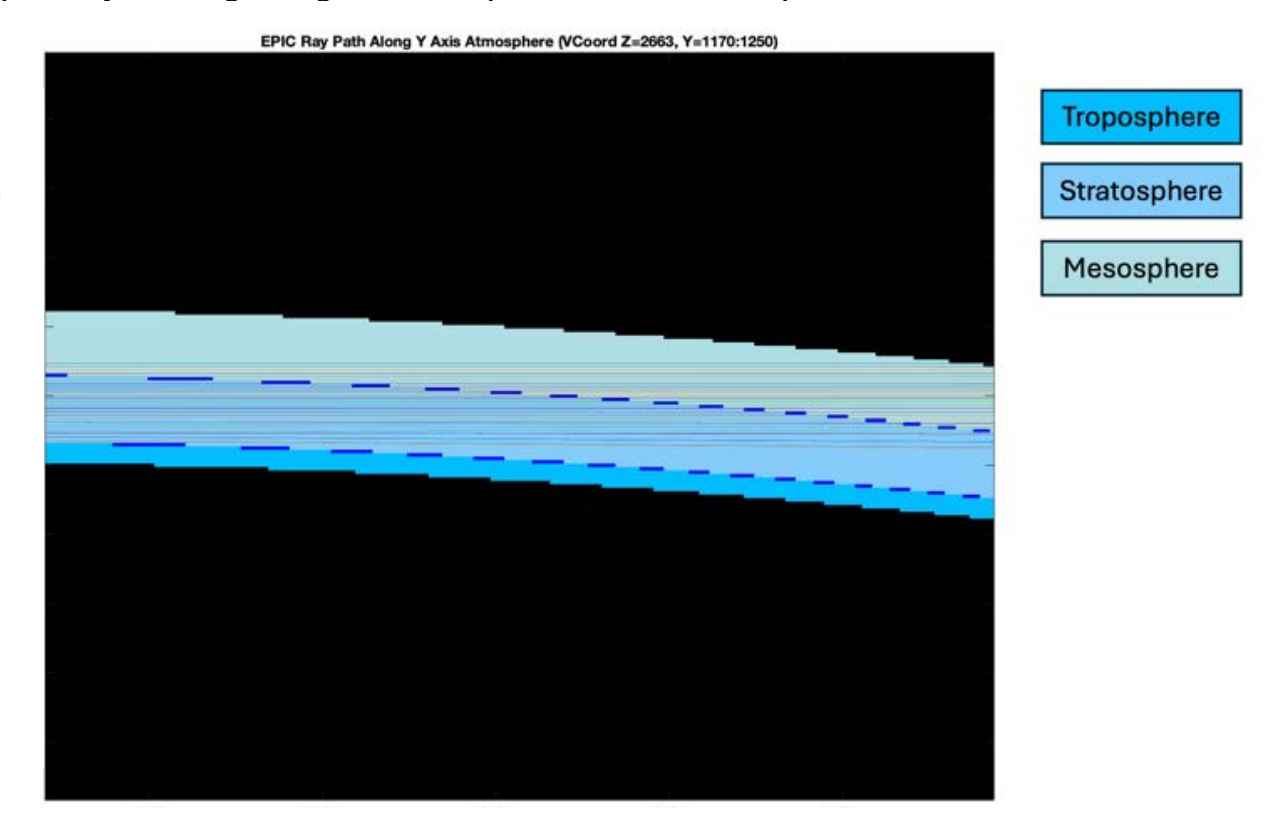


Figure 9 - Illustration of the ray paths. UV light, such as the EPIC 317, 325 and 340nm band as it passes through the stratosphere, would be filtered out by the ozone layers. The rays that hit the troposphere approach the critical angle and are reflected.

This would account for the invisibility of the phenomenon in UV light, as the light passes through the stratosphere (15-30km) it would be filtered out by the ozone layer. The rays that hit the troposphere approach the critical angle and are reflected.

Viewing the full ray paths (*Figure 10*) shows the degree of distortion and where the pixels of the phenomenon originate. The small slice of atmosphere and the distortion caused over the 384,400km distance between the Earth and the Moon, generates over a 4,000 km bending of the rays.

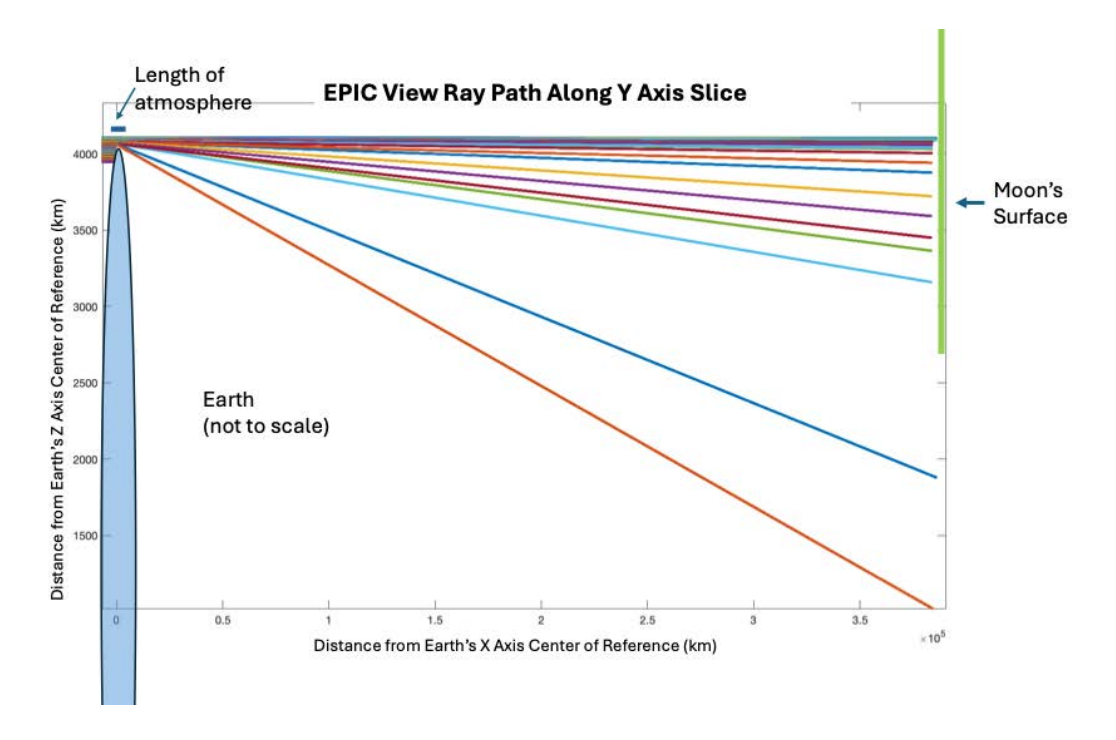


Figure 10 - Slice from raytracer results that shows path of viewing rays and the level of divergence that is caused by atmospheric refraction.

Zooming in on the rays provides more detail in *Figure 11*. Here, several inversions of the light rays can be seen, showing that this phenomenon is not just optical distortion, but a complex mirage. It is interesting to note that while the appearance of the flange is similar to an "omega mirage", the effect is obtained through different means.

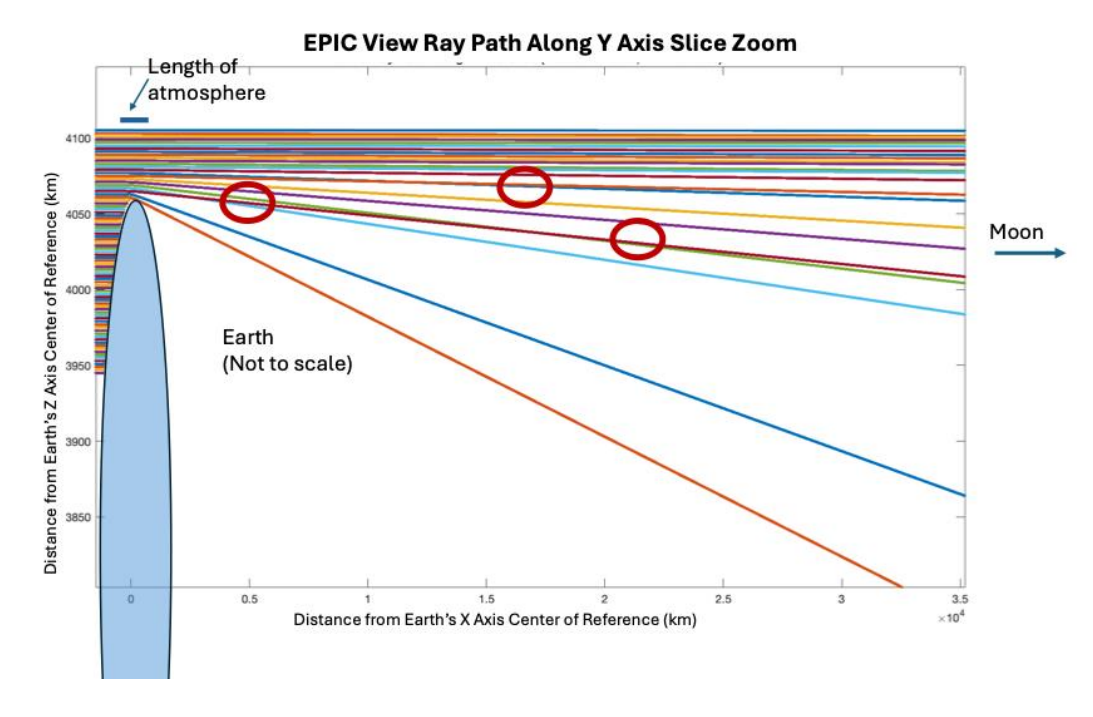


Figure 11 - Zoomed in view of rays. Several ray inversions (circled in red) are seen, indicating a complex mirage.

Inspection of the rays along the Z-axis yields a different picture. Here, the magnitude of distortion is less, but with much greater variance along the slice.

Viewing the rays shows a much more complex distortion in the horizontal vs vertical axis. A zoomed in view shows much more mirage-like ray inversions.

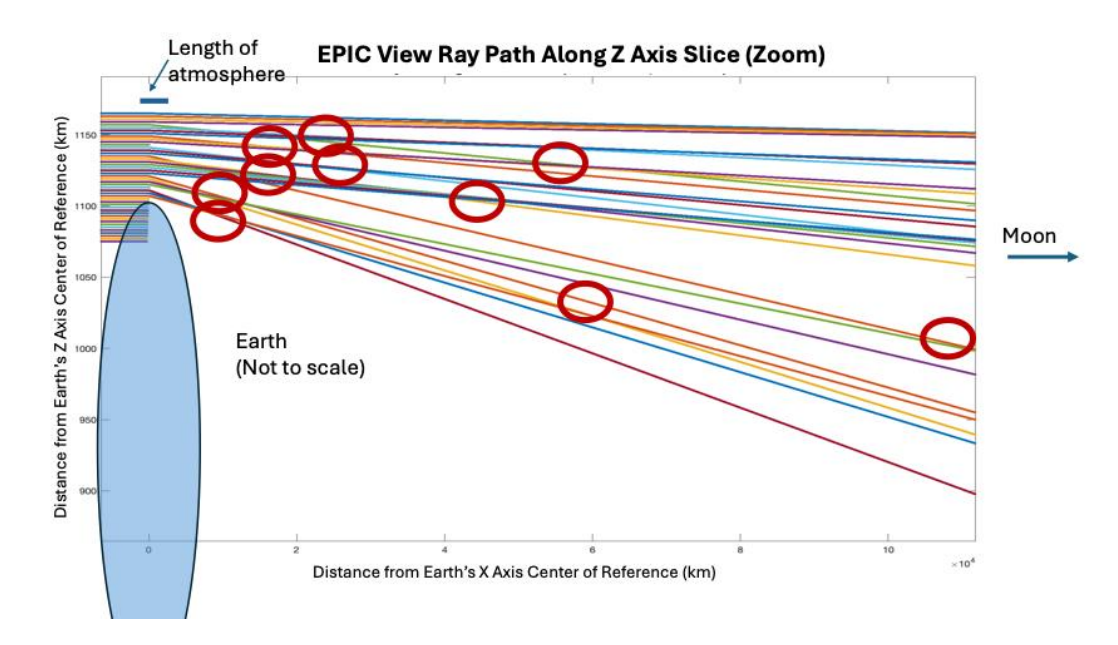


Figure 12 - Zoomed in view of Z-axis slice. Many ray inversions (circled in red) are seen, indicating a complex mirage.

While the analysis shows that the phenomenon is a complex mirage, it does not demonstrate why this phenomenon is visible from EPIC, but not in images closer to the Earth, such as those from GOES or the ISS. In those, the much more expected optical compression effect occurs.

7 Comparative Analysis

In order to determine how the GOES scene differs from EPIC, it is necessary to run the raytracer from the GOES point of view. The GOES ABI has a 17.76° field of view, and by initializing the first vectors with corresponding offsets, it is possible to create a GOES model of the scene.

Running the raytracer for GOES produced the matching optical compressive effect, as seen in *Figure 13*. When viewing the magnitudes of distortion, the degree of distortion is in correlation to the density of the atmosphere according to altitude. Unlike as seen in the EPIC data, there are no "bumps" or aberrations that cause the ray inversions. This is true of both the vertical and horizontal slices. Unlike the EPIC phenomenon, this is not a complex mirage.

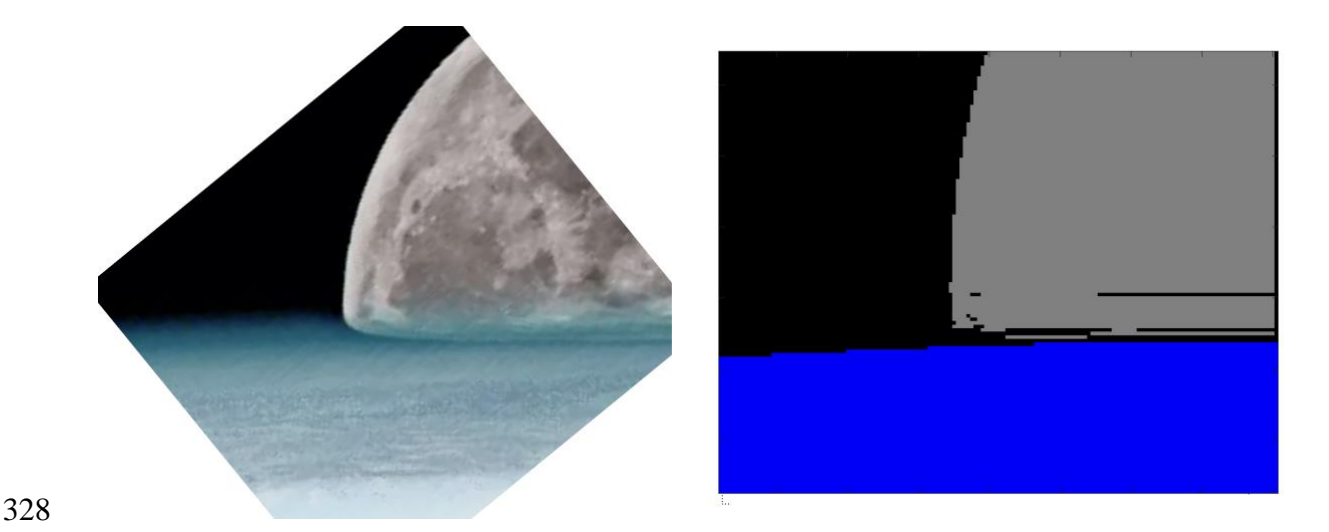


Figure 13 - Left: GOES ABI image showing atmospheric distortion. Right: Simulated scene from raytracer, showing similar effect. Because this model uses discrete rays, small black dots occur where there is no ray present due to diversion from refraction.

What is happening in the EPIC image that is different from GOES? How can two pictures of the same apparent scene cause different optical phenomenon? The answer lies in the fact that although the images appear similar, that similarity is itself an illusion.

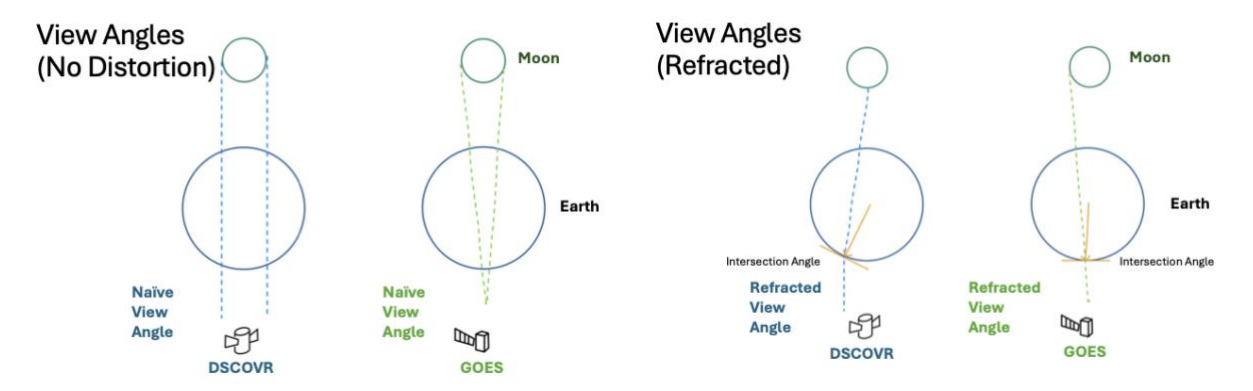
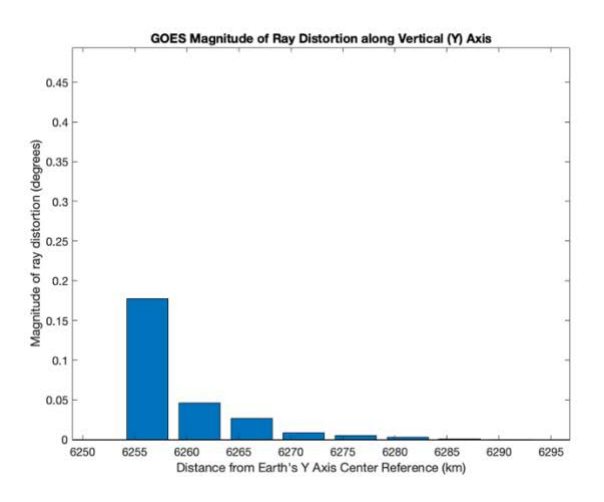


Figure 14 - Left: View angles without distortion. Right: View angles with atmospheric refraction distortion. The different entry angles for the rays on a sphere causes different effects.

DSCOVR orbits the Earth-Sun Lagrange-1 point at over 1.5 million kilometers away from the Earth. To take the pictures requires a telescope with a 0.62° field of view. GOES, on the other hand is in geostationary orbit, a relatively cozy 35 thousand kilometers away from the Earth. In order to get the entire Earth in a single frame requires the instrument to image at a wide angle of 17.76°. This influences the scene; when the Moon is visible to EPIC, it is obscured by the Earth for GOES. In order to do the simulation required shifting the Moon upwards until it was in a similar frame as for EPIC.

When considering the angles and slice of the atmosphere the two instruments view the scene, EPIC's view is across a much wider swath of the atmosphere, while GEOS's is a narrow section near the center (*Figure 14*). This changes the entry angles of the rays; the more extreme angle for EPIC causes a corollary increase in magnitude of refraction, which causes a more extreme reaction when the ray collides with the different refractive indices. This is why the mirage phenomenon occurs with EPIC, but not in GOES or other closer to Earth platforms, such as ISS or other lower orbit satellites.



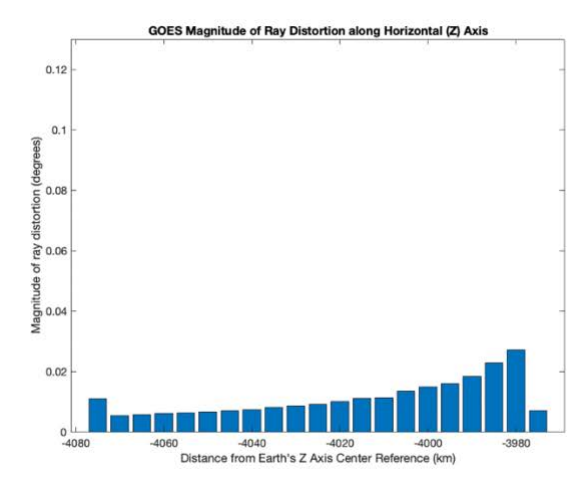


Figure 15 - GOES ABI simulated magnitudes of refractive distortion. Left: Angular distortion of rays on horizontal axis. Right: Angular distortion of rays on vertical axis. Distances are negative since they are left of the center coordinate.

8 Conclusion

The findings demonstrate that the phenomenon seen in the EPIC image when the Moon is at the horizon is a combination of unique atmospheric distortion effects and a complex mirage caused by regular differences in temperature in the atmospheric layers. This phenomenon, "Gaia's Crown", a flange between the Earth and the Moon when the when the two visually intersect, can only be seen in deep space due to larger viewing angles, causing greater distortion because of atmospheric refraction. The demonstrated sensitivity to refraction and high-altitude temperature inversions hints that L1 observations could provide a coarse probe of atmospheric structure.

Author Contributions

KB designed the solutions discussed and wrote the software and the majority of the paper. JK, SD, AM were involved in the validation of technique and identifying issues that needed to be resolved. SD and AT brought attention to the images. All authors contributed to manuscript revision, read and approved the submitted version.

10 Acknowledgments

The work utilized the DSCOVR/EPIC data, which utilizes computational resources and services provided by the NASA Center for Climate Simulation (NCCS) at the Goddard Space Flight Center.

11 Data Availability Statement

370 DSCOVR/EPIC color images can be obtained from https://epic.gsfc.nasa.gov 371 DSCOVR/EPIC science data can be found at https://search.earthdata.nasa.gov/ GEOS data can be obtained from https://gmao.gsfc.nasa.gov 372 373 12 References Angel, E. (2000). Interactive Computer Graphics: A Top-Down Approach with OpenGL. 2nd Edition. 374 375 New York: Addison Wesley Longman, Inc. 376 377 Astronomy.com "A distorted view of a full Moon intersecting Earth's horizon was photographed 378 from the International Space Station. Credit: NASA". Last modified September 7, 2023. 379 https://www.astronomy.com/observing/everything-you-need-to-know-about-the-Moon/ 380 381 Blank, K. (2019). EPIC Geolocation and Color Imagery Algorithm Revision 6. 382 https://asdc.larc.nasa.gov/documents/dscovr/DSCOVR EPIC Geolocation V03.pdf 383 384 Global Modeling Assimilation Office: File Specification for GEOS-5 FP (Forward Processing). 385 January 24, 2017. https://gmao.gsfc.nasa.gov/pubs/docs/Lucchesi1202.pdf 386 MadSci. "The speed of light as a function of air density". Last modified February 26, 1998. 387 388 https://www.madsci.org/posts/archives/feb98/888690999.Ph.r.html 389 390 Marshak, A., J. Herman, A. Szabo, et al. 2018. Earth Observations from DSCOVR/EPIC Instrument. 391 Bulletin Amer. Meteor. Soc. (BAMS), 9, 1829-1850, https://doi.org/10.1175/BAMS-D-17-0223.1. 392 393 Naylor, J. (2002) Out of the Blue: A 24-hour Skywatcher's Guide. New York: Cambridge University 394 Press. 395 396 Nishihama, M., Wolfe, R., Solomon, D., et al. "MODIS Level 1A Earth Location: Algorithm 397 Theoretical Basis Document Version 3.0". Last modified August 26, 1997. https://modis.gsfc.nasa.gov/data/atbd/atbd mod28 v3.pdf 398

400 401 402	NOAA NESIS. "An Ode to the Moon: How NOAA Satellites Capture Earth's Satellite. Last modified September 30, 2020. https://www.nesdis.noaa.gov/news/ode-the-Moon-how-noaa-satellites-capture-earths-satellite
403	
404	
405 406	OmniCalculator. "Air Density Calculator." Last modified July 30 th , 2024. https://www.omnicalculator.com/physics/air-density
407	
408 409	Siebran van der Werf (2022). Novaya Zemlya effect and Fata Morgana. Raytracing in a spherically non-symmetric atmosphere. Computes Rendus Physique. Institut de France Académie des Sciences
410	
411 412	Thormahlen, I. Straub, J, Grigull, U. (1985). Refractive Index of Water and its Dependence on Wavelength, Temperature, and Density. Journal of Physical and Chemical Reference Data 14, 933.
413	
414 415 416	Universe Space Tech. "The Moon "photobombs" the Earth in the image of a Japanese Satellite." March 10, 2023. https://universemagazine.com/en/the-Moon-photobombs-the-earth-in-the-image-of-a-japanese-satellite/
417	
418 419	Wikipedia. "Basic diagram of the optical illusion. By Ludovica Lorenzelli." Last modified December 1, 2014. https://commons.wikimedia.org/w/index.php?curid=37081455
420	
421 422	Wikipedia. "Schematic diagram explaining Fata Morgana. By Brocken Inaglory." Last modified December 6, 2028. https://commons.wikimedia.org/wiki/File:Fada_morgana_graphnn.JPG
423	
424 425	Wikipedia. "Sunset Inferior Mirage. By Brocken Inaglory." Last modified January 12, 2007. https://commons.wikimedia.org/wiki/File:Sunset_inferio_mirage.jpg
426	
427 428	Wikipedia. "Tetens equation." Last modified April 8 th , 2025. https://en.wikipedia.org/wiki/Tetens_equation
429	